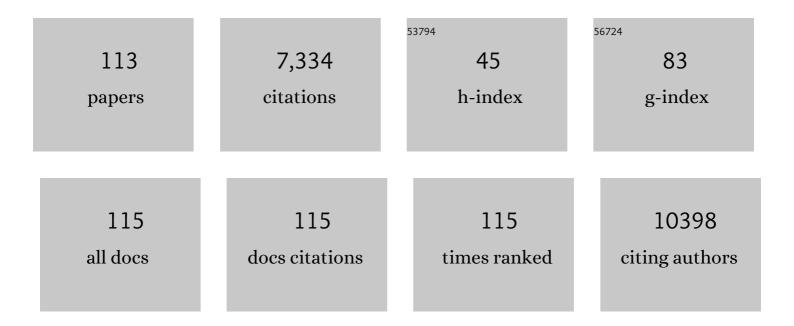
Huimin Zhao

List of Publications by Year in descending order

Source: https://exaly.com/author-pdf/1893920/publications.pdf Version: 2024-02-01



Ηιμμινί Ζηλο

#	Article	IF	CITATIONS
1	Graphene oxide modified g-C ₃ N ₄ hybrid with enhanced photocatalytic capability under visible light irradiation. Journal of Materials Chemistry, 2012, 22, 2721-2726.	6.7	687
2	Facile Ammonia Synthesis from Electrocatalytic N ₂ Reduction under Ambient Conditions on N-Doped Porous Carbon. ACS Catalysis, 2018, 8, 1186-1191.	11.2	520
3	Fabrication of atomic single layer graphitic-C3N4 and its high performance of photocatalytic disinfection under visible light irradiation. Applied Catalysis B: Environmental, 2014, 152-153, 46-50.	20.2	394
4	Interface Engineering Catalytic Graphene for Smart Colorimetric Biosensing. ACS Nano, 2012, 6, 3142-3151.	14.6	270
5	Selective Electrochemical Reduction of Carbon Dioxide to Ethanol on a Boron―and Nitrogenâ€Coâ€doped Nanodiamond. Angewandte Chemie - International Edition, 2017, 56, 15607-15611.	13.8	226
6	TiO ₂ â^'Multiwalled Carbon Nanotube Heterojunction Arrays and Their Charge Separation Capability. Journal of Physical Chemistry C, 2007, 111, 12987-12991.	3.1	222
7	Two-dimensional MoS2: A promising building block for biosensors. Biosensors and Bioelectronics, 2017, 89, 56-71.	10.1	215
8	Selective Electrochemical Reduction of Carbon Dioxide to Ethanol on a Boron―and Nitrogen oâ€doped Nanodiamond. Angewandte Chemie, 2017, 129, 15813-15817.	2.0	196
9	Efficient Mineralization of Perfluorooctanoate by Electro-Fenton with H ₂ O ₂ Electro-generated on Hierarchically Porous Carbon. Environmental Science & Technology, 2015, 49, 13528-13533.	10.0	174
10	Improved Photocatalytic Performance of Heterojunction by Controlling the Contact Facet: High Electron Transfer Capacity between TiO ₂ and the {110} Facet of BiVO ₄ Caused by Suitable Energy Band Alignment. Advanced Functional Materials, 2015, 25, 3074-3080.	14.9	164
11	Roles of magnetite and granular activated carbon in improvement of anaerobic sludge digestion. Bioresource Technology, 2018, 249, 666-672.	9.6	163
12	Evaluation on direct interspecies electron transfer in anaerobic sludge digestion of microbial electrolysis cell. Bioresource Technology, 2016, 200, 235-244.	9.6	157
13	A universal immunosensing strategy based on regulation of the interaction between graphene and graphene quantum dots. Chemical Communications, 2013, 49, 234-236.	4.1	156
14	Atomic single layer graphitic-C ₃ N ₄ : fabrication and its high photocatalytic performance under visible light irradiation. RSC Advances, 2014, 4, 624-628.	3.6	152
15	MoS2 nanostructures for electrochemical sensing of multidisciplinary targets: A review. TrAC - Trends in Analytical Chemistry, 2018, 102, 75-90.	11.4	138
16	A versatile fluorescent biosensor based on target-responsive graphene oxide hydrogel for antibiotic detection. Biosensors and Bioelectronics, 2016, 83, 267-273.	10.1	123
17	Fe ₃ O ₄ -AuNPs anchored 2D metal–organic framework nanosheets with DNA regulated switchable peroxidase-like activity. Nanoscale, 2017, 9, 18699-18710.	5.6	122
18	Degradation of p-nitrophenol in aqueous solution by microwave assisted oxidation process through a granular activated carbon fixed bed. Water Research, 2006, 40, 3061-3068.	11.3	114

#	Article	IF	CITATIONS
19	Facile Method for Fabricating Boron-Doped TiO ₂ Nanotube Array with Enhanced Photoelectrocatalytic Properties. Industrial & Engineering Chemistry Research, 2008, 47, 3804-3808.	3.7	107
20	Enhanced photocatalytic performance of a two-dimensional BiOIO3/g-C3N4 heterostructured composite with a Z-scheme configuration. Applied Catalysis B: Environmental, 2018, 237, 947-956.	20.2	99
21	Three-Dimensional Graphene Supported Bimetallic Nanocomposites with DNA Regulated-Flexibly Switchable Peroxidase-Like Activity. ACS Applied Materials & Interfaces, 2016, 8, 9855-9864.	8.0	89
22	Nanocarbon-based membrane filtration integrated with electric field driving for effective membrane fouling mitigation. Water Research, 2016, 88, 285-292.	11.3	89
23	Boron and Nitrogen Codoped Nanodiamond as an Efficient Metal-Free Catalyst for Oxygen Reduction Reaction. Journal of Physical Chemistry C, 2013, 117, 14992-14998.	3.1	80
24	Porous metal–organic framework MIL-100(Fe) as an efficient catalyst for the selective catalytic reduction of NO _x with NH ₃ . RSC Advances, 2014, 4, 48912-48919.	3.6	80
25	Electrochemical Determination of Tetracycline Using Molecularly Imprinted Polymer Modified Carbon Nanotubeâ€Gold Nanoparticles Electrode. Electroanalysis, 2011, 23, 1863-1869.	2.9	77
26	Stimuli-responsive peroxidase mimicking at a smart graphene interface. Chemical Communications, 2012, 48, 7055.	4.1	76
27	Voltammetric sensing based on the use of advanced carbonaceous nanomaterials: a review. Mikrochimica Acta, 2018, 185, 89.	5.0	67
28	Enhancement of anaerobic methanogenesis at a short hydraulic retention time via bioelectrochemical enrichment of hydrogenotrophic methanogens. Bioresource Technology, 2016, 218, 505-511.	9.6	66
29	Dynamic adsorption of ciprofloxacin on carbon nanofibers: Quantitative measurement by in situ fluorescence. Journal of Water Process Engineering, 2016, 9, e14-e20.	5.6	61
30	Transition metal dichalcogenide-based mixed-dimensional heterostructures for visible-light-driven photocatalysis: Dimensionality and interface engineering. Nano Research, 2021, 14, 2003-2022.	10.4	61
31	A bimetallic Co/Mn metal–organic-framework with a synergistic catalytic effect as peroxidase for the colorimetric detection of H ₂ 0 ₂ . Analytical Methods, 2019, 11, 1111-1124.	2.7	60
32	Efficient visible-light activation of molecular oxygen to produce hydrogen peroxide using P doped g-C ₃ N ₄ hollow spheres. Journal of Materials Chemistry A, 2020, 8, 22720-22727.	10.3	59
33	Covalent functionalization of MoS2 nanosheets synthesized by liquid phase exfoliation to construct electrochemical sensors for Cd (II) detection. Talanta, 2018, 182, 38-48.	5.5	58
34	Fluorescent assay for oxytetracycline based on a long-chain aptamer assembled onto reduced graphene oxide. Mikrochimica Acta, 2013, 180, 829-835.	5.0	57
35	A visible and label-free colorimetric sensor for miRNA-21 detection based on peroxidase-like activity of graphene/gold-nanoparticle hybrids. Analytical Methods, 2016, 8, 2005-2012.	2.7	57
36	Reduction of acute toxicity and genotoxicity of dye effluent using Fenton-coagulation process. Journal of Hazardous Materials, 2014, 274, 198-204.	12.4	54

#	Article	IF	CITATIONS
37	Effects of developmental perfluorooctane sulfonate exposure on spatial learning and memory ability of rats and mechanism associated with synaptic plasticity. Food and Chemical Toxicology, 2015, 76, 70-76.	3.6	54
38	Preparation of Zn-doped TiO2 nanotubes electrode and its application in pentachlorophenol photoelectrocatalytic degradation. Science Bulletin, 2007, 52, 1456-1461.	1.7	52
39	Controllable oxidative DNA cleavage-dependent regulation of graphene/DNA interaction. Chemical Communications, 2011, 47, 4084.	4.1	50
40	An electrochemical sensor for selective determination of sulfamethoxazole in surface water using a molecularly imprinted polymer modified BDD electrode. Analytical Methods, 2015, 7, 2693-2698.	2.7	50
41	Impact of dissolved organic matter on the photolysis of the ionizable antibiotic norfloxacin. Journal of Environmental Sciences, 2015, 27, 115-123.	6.1	50
42	Two-dimensional nanomaterial based sensors for heavy metal ions. Mikrochimica Acta, 2018, 185, 478.	5.0	48
43	Electrochemical Preparation of Gold Nanoparticles-Polypyrrole Co-Decorated 2D MoS ₂ Nanocomposite Sensor for Sensitive Detection of Glucose. Journal of the Electrochemical Society, 2019, 166, B147-B154.	2.9	48
44	Enhanced adsorption of ionizable antibiotics on activated carbon fiber under electrochemical assistance in continuous-flow modes. Water Research, 2018, 134, 162-169.	11.3	47
45	Amphiphilic PA-induced three-dimensional graphene macrostructure with enhanced removal of heavy metal ions. Journal of Colloid and Interface Science, 2018, 512, 853-861.	9.4	47
46	A colorimetric aptasensor for sulfadimethoxine detection based on peroxidase-like activity of graphene/nickel@palladium hybrids. Analytical Biochemistry, 2017, 525, 92-99.	2.4	46
47	Bimetallic Fe/Mn metal-organic-frameworks and Au nanoparticles anchored carbon nanotubes as a peroxidase-like detection platform with increased active sites and enhanced electron transfer. Talanta, 2020, 210, 120678.	5.5	45
48	A graphene and multienzyme functionalized carbon nanosphere-based electrochemical immunosensor for microcystin-LR detection. Colloids and Surfaces B: Biointerfaces, 2013, 103, 38-44.	5.0	44
49	DNA-modified graphene quantum dots as a sensing platform for detection of Hg ²⁺ in living cells. RSC Advances, 2015, 5, 39587-39591.	3.6	43
50	PEGylated molybdenum dichalcogenide (PEG-MoS ₂) nanosheets with enhanced peroxidase-like activity for the colorimetric detection of H ₂ O ₂ . New Journal of Chemistry, 2017, 41, 6700-6708.	2.8	42
51	Multiple application of SAzyme based on carbon nitride nanorod-supported Pt single-atom for H2O2 detection, antibiotic detection and antibacterial therapy. Chemical Engineering Journal, 2022, 427, 131572.	12.7	42
52	Photoelectrochemical immunoassay for microcystin-LR based on a fluorine-doped tin oxide glass electrode modified with a CdS-graphene composite. Mikrochimica Acta, 2012, 179, 163-170.	5.0	39
53	Three-Dimensional Porous H _{<i>x</i>} TiS ₂ Nanosheet–Polyaniline Nanocomposite Electrodes for Directly Detecting Trace Cu(II) Ions. Analytical Chemistry, 2015, 87, 5605-5613.	6.5	39
54	Photoelectrochemical aptasensor for sulfadimethoxine using g-C3N4 quantum dots modified with reduced graphene oxide. Mikrochimica Acta, 2018, 185, 345.	5.0	38

#	Article	IF	CITATIONS
55	2D Ti3C2Tx flakes prepared by in-situ HF etchant for simultaneous screening of carbamate pesticides. Journal of Colloid and Interface Science, 2021, 590, 365-374.	9.4	38
56	Visible assay for glycosylase based on intrinsic catalytic ability of graphene/gold nanoparticles hybrids. Biosensors and Bioelectronics, 2015, 68, 7-13.	10.1	37
57	Electrochemical reduction of carbon dioxide to formate with Fe-C electrodes in anaerobic sludge digestion process. Water Research, 2016, 106, 339-343.	11.3	37
58	In situ controllable growth of noble metal nanodot on graphene sheet. Journal of Materials Chemistry, 2011, 21, 12986.	6.7	36
59	Photochemical Formation of Hydroxylated Polybrominated Diphenyl Ethers (OH-PBDEs) from Polybrominated Diphenyl Ethers (PBDEs) in Aqueous Solution under Simulated Solar Light Irradiation. Environmental Science & Technology, 2015, 49, 9092-9099.	10.0	35
60	Effects of perfluorooctane sulfonate and its alternatives on long-term potentiation in the hippocampus CA1 region of adult rats in vivo. Toxicology Research, 2016, 5, 539-546.	2.1	35
61	Fluorescent biosensor for sensitive analysis of oxytetracycline based on an indirectly labelled long-chain aptamer. RSC Advances, 2015, 5, 58895-58901.	3.6	32
62	Enhanced photocatalytic degradation of tetracycline hydrochloride by molecular imprinted film modified TiO2 nanotubes. Science Bulletin, 2012, 57, 601-605.	1.7	30
63	Three-Dimensional Branched Crystal Carbon Nitride with Enhanced Intrinsic Peroxidase-Like Activity: A Hypersensitive Platform for Colorimetric Detection. ACS Applied Materials & Interfaces, 2019, 11, 17467-17474.	8.0	29
64	Propagation of antibiotic resistance genes in an industrial recirculating aquaculture system located at northern China. Environmental Pollution, 2020, 261, 114155.	7.5	29
65	Recent advances and perspectives of enzyme-based optical biosensing for organophosphorus pesticides detection. Talanta, 2022, 240, 123145.	5.5	29
66	Signal amplified photoelectrochemical assay based on Polypyrrole/g-C3N4/WO3 inverse opal photonic crystals triple heterojunction assembled through sandwich-type recognition model. Sensors and Actuators B: Chemical, 2020, 310, 127888.	7.8	27
67	A ZIF-8-based platform for the rapid and highly sensitive detection of indoor formaldehyde. RSC Advances, 2014, 4, 36444-36450.	3.6	26
68	Determination of Oxytetracycline by a Graphene—Gold Nanoparticle-Based Colorimetric Aptamer Sensor. Analytical Letters, 2017, 50, 544-553.	1.8	26
69	Understanding signal amplification strategies of nanostructured electrochemical sensors for environmental pollutants. Current Opinion in Electrochemistry, 2019, 17, 56-64.	4.8	26
70	Gold modified microelectrode for direct tetracycline detection. Frontiers of Environmental Science and Engineering, 2012, 6, 313-319.	6.0	23
71	Photochemical transformation of 2,2′,4,4′-tetrabromodiphenyl ether (BDE-47) in surface coastal waters: Effects of chloride and ferric ions. Marine Pollution Bulletin, 2014, 86, 76-83.	5.0	23
72	Electrochemical Biosensor for Detection of Perfluorooctane Sulfonate Based on Inhibition Biocatalysis of Enzymatic Fuel Cell. Electrochemistry, 2014, 82, 94-99.	1.4	22

#	Article	IF	CITATIONS
73	Poly(vinylidene fluoride) hollowâ€fiber membranes containing silver/graphene oxide dope with excellent filtration performance. Journal of Applied Polymer Science, 2017, 134, .	2.6	21
74	Preparation of 3D assembly of mono layered molybdenum disulfide nanotubules for rapid screening of carbamate pesticide diethofencarb. Talanta, 2019, 204, 455-464.	5.5	21
75	Signal amplified photoelectrochemical sensing platform with g-C3N4/inverse opal photonic crystal WO3 heterojunction electrode. Journal of Electroanalytical Chemistry, 2019, 840, 101-108.	3.8	20
76	3D V2O5-MoS2/rGO nanocomposites with enhanced peroxidase mimicking activity for sensitive colorimetric determination of H2O2 and glucose. Spectrochimica Acta - Part A: Molecular and Biomolecular Spectroscopy, 2022, 269, 120750.	3.9	20
77	Enhanced Photocatalytic Production of H ₂ O ₂ through Regulation of Spatial Charge Transfer and Light Absorption over a MnIn ₂ S ₄ /WO ₃ (Yb,) Tj ETQq1	₫. ₽.7843	1240rgBT /Ov
78	Catalytic hairpin assembly indirectly covalent on Fe3O4@C nanoparticles with signal amplification for intracellular detection of miRNA. Talanta, 2021, 223, 121675.	5.5	19
79	Developmental perfluorooctane sulfonate exposure results in tau hyperphosphorylation and β-amyloid aggregation in adults rats: Incidence for link to Alzheimer's disease. Toxicology, 2016, 347-349, 40-46.	4.2	18
80	An Electrochemical Sensor based on p-aminothiophenol/Au Nanoparticle-Decorated H TiS2 Nanosheets for Specific Detection of Picomolar Cu (II). Electrochimica Acta, 2016, 190, 480-489.	5.2	18
81	Extending suitability of physisorption strategy in fluorescent platforms design: Surface passivation and covalent linkage on MOF nanosheets with enhanced OTC detection sensitivity. Sensors and Actuators B: Chemical, 2020, 303, 127230.	7.8	18
82	Selection and characterization of DNA aptamers for constructing colorimetric biosensor for detection of PBP2a. Spectrochimica Acta - Part A: Molecular and Biomolecular Spectroscopy, 2020, 228, 117735.	3.9	18
83	Electrochemically enhanced adsorption of PFOA and PFOS on multiwalled carbon nanotubes in continuous flow mode. Science Bulletin, 2014, 59, 2890-2897.	1.7	17
84	Enhanced Photodegradation of PNP on Soil Surface under UV Irradiation with TiO2. Soil and Sediment Contamination, 2007, 16, 413-421.	1.9	16
85	Tuning the electrochemical properties of a boron and nitrogen codoped nanodiamond rod array to achieve high performance for both electro-oxidation and electro-reduction. Journal of Materials Chemistry A, 2013, 1, 14706.	10.3	16
86	Enhanced Electrochemiluminescence Detection for Hydrogen Peroxide Using Peroxidase-Mimetic Fe/N-Doped Porous Carbon. Journal of the Electrochemical Society, 2019, 166, B1594-B1601.	2.9	16
87	Preparation and characterization of aligned carbon nanotubes coated with titania nanoparticles. Science Bulletin, 2006, 51, 2294-2296.	1.7	14
88	Voltage-Gated Transport of Nanoparticles across Free-Standing All-Carbon-Nanotube-Based Hollow-Fiber Membranes. ACS Applied Materials & Interfaces, 2015, 7, 14620-14627.	8.0	14
89	Enhancement of sludge granulation in hydrolytic acidogenesis by denitrification. Applied Microbiology and Biotechnology, 2016, 100, 3313-3320.	3.6	14
90	Real Time Detection of Hazardous Hydroxyl Radical Using an Electrochemical Approach. ChemistrySelect, 2019, 4, 12507-12511.	1.5	14

#	Article	IF	CITATIONS
91	Environmental and intercellular Pb2+ ions determination based on encapsulated DNAzyme in nanoscale metal-organic frameworks. Mikrochimica Acta, 2020, 187, 608.	5.0	14
92	Perfluorooctane sulfonate induces apoptosis of hippocampal neurons in rat offspring associated with calcium overload. Toxicology Research, 2015, 4, 931-938.	2.1	12
93	Fabrication of needle-like ZnO nanorods arrays by a low-temperature seed-layer growth approach in solution. Applied Physics A: Materials Science and Processing, 2007, 89, 673-679.	2.3	11
94	Non enzymatic fluorometric determination of glucose by using quenchable g-C3N4 quantum dots. Mikrochimica Acta, 2019, 186, 779.	5.0	10
95	Developmental perfluorooctane sulfonate exposure inhibits long-term potentiation by affecting AMPA receptor trafficking. Toxicology, 2019, 412, 55-62.	4.2	10
96	Signal amplified sandwich-type photoelectrochemical sensing assay based on rGO-Znln2S4 functionalized Au–WO3 IOPCs Z-scheme heterojunction. Electrochimica Acta, 2021, 365, 137382.	5.2	10
97	Ultrasensitive immunoassay of microcystins-LR using G-quadruplex DNAzyme as an electrocatalyst. International Journal of Environmental Analytical Chemistry, 2014, 94, 988-1000.	3.3	9
98	Electrochemical Oxidation of Tannic Acid at ZIF-8 Induced Nitrogen Doped Porous Carbon Nanoframework Modified Electrode. Journal of the Electrochemical Society, 2018, 165, H1004-H1011.	2.9	9
99	Prevalence of antibiotic resistance genes in wastewater collected from ornamental fish market in northern China. Environmental Pollution, 2021, 271, 116316.	7.5	9
100	Electrocatalytic dechlorination of 2,4,5-trichlorobiphenyl using an aligned carbon nanotubes electrode deposited with palladium nanoparticles. Science Bulletin, 2010, 55, 358-364.	1.7	8
101	A strategy for enhancing anaerobic digestion of waste activated sludge: Driving anodic oxidation by adding nitrate into microbial electrolysis cell. Journal of Environmental Sciences, 2019, 81, 34-42.	6.1	8
102	<scp>WO₃</scp> Inversce Opal Photonic Crystals: Unique Property, Synthetic Methods and Extensive Application. Chinese Journal of Chemistry, 2021, 39, 1706-1715.	4.9	8
103	Enhancing nitrogen removal efficiency in a dyestuff wastewater treatment plant with the IFFAS process: the pilot-scale and full-scale studies. Water Science and Technology, 2018, 77, 70-78.	2.5	7
104	CNT-Modified MIL-88(NH2)-Fe for Enhancing DNA-Regulated Peroxidase-Like Activity. Journal of Analysis and Testing, 2019, 3, 238-245.	5.1	7
105	Salt-controlled assembly of stacked-graphene for capturing fluorescence and its application in chemical genotoxicity screening. Journal of Materials Chemistry, 2011, 21, 15266.	6.7	6
106	Coupling O ₂ and K ₂ S ₂ O ₈ Dual Coâ€reactant with Feâ€N Modified Electrode for Ultrasensitive Electrochemiluminescence Signal Amplification. ChemistrySelect, 2019, 4, 1673-1680.	2 1.5	5
107	Highly sensitive detection of salvianic acid a drug by a novel electrochemical sensor based on HKUST-1 loaded on three-dimensional graphene-MWCNT composite. Journal of Pharmaceutical and Biomedical Analysis, 2021, 206, 114389.	2.8	5
108	Activating the Basal Planes in 2Hâ€MoTe ₂ Monolayers by Incorporating Singleâ€Atom Dispersed N or P for Enhanced Electrocatalytic Overall Water Splitting. Advanced Sustainable Systems, 2022, 6, .	5.3	4

#	Article	IF	CITATIONS
109	Sensitive detection of quorum signaling molecules (<i>N</i> -acyl homoserine lactones) in activated sludge based on surface molecularly imprinted polymers on CQDs@MIL-101. Environmental Science: Water Research and Technology, 2022, 8, 1211-1222.	2.4	2
110	Adsorption performance and its mechanism of aqueous As (III) on polyporous calcined oyster shellâ€supported Feâ€Mn binary oxide. Water Environment Research, 2022, 94, e10714.	2.7	2
111	Influence of Temperature and Oil Content on the Soil/Air Partition Coefficient for Hexachlorobenzene in Oil-Contaminated Rice Paddy Field Soil. Soil and Sediment Contamination, 2011, 20, 221-233.	1.9	1
112	Innentitelbild: Selective Electrochemical Reduction of Carbon Dioxide to Ethanol on a Boron―and Nitrogen oâ€doped Nanodiamond (Angew. Chem. 49/2017). Angewandte Chemie, 2017, 129, 15678-15678.	2.0	1
113	Ultrasensitive sandwich-type photoelectrochemcial oxytetracycline sensing platform based on MnIn2S4/WO3 (Yb, Tm) functionalized rGO film. Journal of Electroanalytical Chemistry, 2022, 915, 116354.	3.8	1